

# Confinement and Activity-Driven Dynamics of Semiflexible Polymers in Motility Assays

Sandip Roy\* and Anil Kumar Dasanna†

*Indian Institute of Science Education and Research Mohali,  
Knowledge City, Sector 81, SAS Nagar 140306, Punjab, India*

(Dated: January 8, 2025)

We investigate the dynamics of semiflexible polymers in a motility assay, where motor proteins (MPs) stochastically bind, unbind, and walk along the polymer, under the influence of harmonic confinement. Using Langevin dynamics simulations, we explore the interplay between the polymer's rigidity, activity in the form of attachment/detachment of MPs and subsequent movement of attached MPs, and trap strength, revealing a two-state transition from a trapped to a free polymer, with an intermediate coexistence region. Rigidity significantly impacts the trapping behaviour, with flexible polymers remaining trapped at the higher activity. Attachment/detachment of MPs can also induce a change in the effective rigidity of the polymer and, therefore, influence confinement by the trap. We show that confinement stabilizes spiral structures and suppresses open-chain motion, especially at higher activity. The centre of mass (COM) dynamics are analyzed through the mean square displacement (MSD), showing diffusive, ballistic, and diffusive regimes that depend on the trap strength and activity. Negative excess kurtosis indicates nonequilibrium behaviour, which saturates with increasing confinement, reflecting the dominance of the trap over the activity.

## I. INTRODUCTION

The cytoskeleton plays a crucial role in preserving the cell's structure. It is composed of a complex and dynamic network of interconnected protein polymers within the cytoplasm. Basically, it includes three types of filaments: micropolymers, intermediate filaments, and microtubules, on the order of increasing filament size. Among the three, actin has the shortest persistence length, about  $17 \mu\text{m}$  and microtubules have the longest persistence length of around a few millimeters [1]. All of these filaments can be dynamically assembled or disassembled on their respective time and length scales according to the cell's requirements [2] and often their dynamic behavior is closely coordinated by motor proteins that are responsible for the major active transport inside the cell. They use the energy from ATP hydrolysis to move along the filaments. In many biological processes, myosin polymers are often associated with actin filaments, while dynein and kinesin are associated with microtubules [3]. Some motor proteins also instigate the motion of cytoskeletal filaments relative to each other, producing the force necessary for crucial cellular functions such as muscle contraction, ciliary beating, and cell division [4].

In vitro motor protein assay provides a useful platform for probing polymer-motor dynamics in detail, where motor proteins grafted onto a coverslip apply tangential forces along the polymer in the presence of ATP [5–7]. This motility set-up has also been exploited in theoretical analysis and computer simulations, and such a polymer has been shown to display variety of dynamical behavior such as spiral formation, collective gliding and swirling [8–13]. Such spiral formation has also

been observed in polar active polymers, where an active force acts along the tangent of the polymer [14]. Recently, it has been shown that the actively driven polymer fixed at one end of the motor bed induces rotation and beating motion, which is reminiscent of the ciliary motion [15]. More intricate ciliary movements, including traveling waves and synchronized oscillations, are also effectively captured by arrays of polar active filaments that are anchored at one end. [16–18].

The confinement of living microorganisms and self-propelled particles using external traps provides a vital tool for analyzing the motion and behavior of dynamic systems [19–24]. Among these, optical traps, commonly known as optical tweezers, have been widely employed to study various properties of motility assays and the organisms themselves. For example, optical tweezers have been used to investigate dynamic structural changes associated with the ATPase cycle [25] of motor proteins, protein folding-unfolding [26], excitement and transformation of lipid-bilayer [27], bacterial twitching motility [28], the flexural rigidity of actin polymers [29], bacterial swimming manipulation [30], and sperm motility [31]. These studies highlight the versatility of optical tweezers in probing microscopic systems. In particular, polymer trapping in a region smaller than its radius of gyration offers a useful framework to understand the packing of chromosomes within the nucleus [32]. Although equilibrium properties can be derived using scaling arguments [33, 34], dynamical properties have gained particular interest in a variety of contexts. These include translocation through pores [35–39], diffusion through networks and tubes, and DNA packing within viral capsids [40, 41]. However, few studies have focused on the trapping of polymers, such as semi-flexible polymers, in active motility assays using optical traps. Such studies could provide insight into the dynamics of polymers under external confinement, which is essential to understand both biological processes and synthetic systems.

\* mp16001@iisermohali.ac.in

† adasanna@iisermohali.ac.in

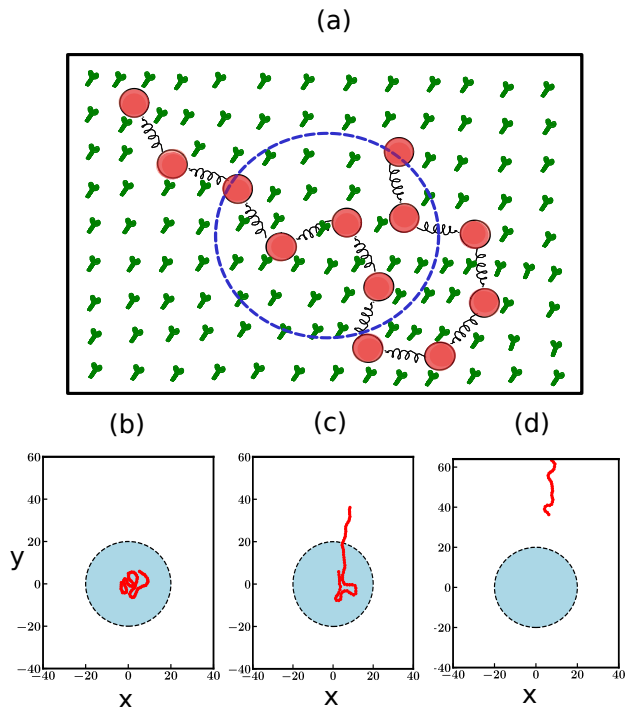


FIG. 1: (a) Schematic depiction of the system, showcasing motor proteins organized on a square grid (green). The semiflexible polymer is shown as a bead-spring chain (red) and positioned on the grid, with many MPs affixed to it. A blue circle near the middle of the grid denotes the region of harmonic confinement. Snapshots depicting the time evolution of a semiflexible polymer (red) with a contour length of  $L = 63\sigma$ , a stiffness parameter  $\ell_p/L = 0.3$ , bare processivity  $\Omega = 0.5$ , and a Péclet number of  $Pe = 9.9 \times 10^4$ , placed within a harmonic trap (blue) defined by a trap radius of  $\mathcal{R} = 20\sigma$  and a trap strength of  $K_{\text{trap}} = 0.05k_B T/\sigma^2$ . Panel (a) illustrates the initial condition at  $t = 0$ , where the polymer is entirely contained within the trap. Panel (b) depicts an intermediate time point, demonstrating the polymer gradually moving out of the trap, leading to a partial trapping situation. Panel (c) illustrates a subsequent time period in which the polymer has entirely evaded the trap.

The current study presents a comprehensive two-dimensional motility assay model that analyzes the morphological and dimensional transformations of an extensible semi-flexible polymer propelled by motor proteins within a localized harmonic trap delineated by a specified trap radius. In our framework, the motor protein tails are anchored to the substrate, while their heads can attach and detach from the polymer, facilitating its active extension. In the following sections, we first present our model and then we present a state diagram consisting of primarily bound and unbound state. We will also discuss how this state diagram changes for various activities, motor kinetic rates, and trap strength. In subsequent sections, we further explore the dynamics including mean-square displacement, spiral number, and kurtosis.

## II. MODEL AND THEORY

We model a semi-flexible polymer consisting of  $N$  beads, with a total length  $L = (N - 1)\sigma$ ; where  $\sigma$  is the equilibrium bond length. A stretching potential describes the interaction between adjacent beads:

$$V_s = \sum_{i=1}^{N-1} \frac{K}{2\sigma} [\vec{\mathbf{b}}_i - \sigma \hat{\mathbf{t}}_i]^2 \quad (1)$$

where  $\mathbf{b}_i = \mathbf{r}_{i+1} - \mathbf{r}_i$  is the bond vector and  $\hat{\mathbf{t}}_i = \mathbf{b}_i/b_i$  is the unit tangent vector, with  $K$  the bond stiffness. The bending resistance between consecutive tangent vectors  $\hat{\mathbf{t}}_i$  and  $\hat{\mathbf{t}}_{i+1}$  is given by

$$V_b = \sum_{i=1}^{N-2} \frac{\kappa}{2\sigma} [\hat{\mathbf{t}}_{i+1} - \hat{\mathbf{t}}_i]^2 \quad (2)$$

where  $\kappa$  is the bending rigidity and the persistence length  $\ell_p = 2\kappa/(d-1)k_B T$  quantifies the polymer stiffness in  $d$ -dimensions [42, 43].

Excluded volume interactions between non-bonded pairs are modelled using the Weeks-Chandler-Anderson (WCA) potential:

$$V_{WCA} = \begin{cases} 4\epsilon \left[ \left( \frac{\sigma}{r_{ij}} \right)^{12} - \left( \frac{\sigma}{r_{ij}} \right)^6 + \frac{1}{4} \right], & \text{if } r_{ij} < 2^{\frac{1}{6}}\sigma \\ 0, & \text{otherwise} \end{cases} \quad (3)$$

The total energy is then given by  $V = V_s + V_b + V_{WCA}$ .

The polymer is placed on a substrate with motor proteins (MPs) distributed in a two-dimensional grid. MPs can bind to a polymer bead within a capture radius  $r_c$  with an on-rate  $\kappa_{\text{on}}$ . Once bound, they exert a force  $\mathbf{f}_i = -k_m \Delta \mathbf{r}$  on the polymer, with elongation due to two processes: (1) the attached MP being pulled with the polymer, and (2) active motion along the polymer with velocity

$$v_t^a = \frac{v_0}{1 + d_0 \exp(\frac{f_t}{f_s})}. \quad (4)$$

The force  $\mathbf{f}_i$  is distributed between the adjacent monomers according to the lever rule. MP binds to the polymer with a constant onrate  $\kappa_{\text{on}}$  when the distance is less than  $0.5\sigma$ . The unbinding kinetics follow Bell's law [44]:

$$\kappa_{\text{off}} = \kappa_0 \exp\left(\frac{f_t}{f_d}\right) \quad (5)$$

where  $f_t = |\mathbf{f}_i|$  is the force on the polymer,  $\kappa_0$  is unstressed offrate and  $f_d$  is the force scale which depends on the nature of the bond. The active velocity along the polymer is:

$$v_t^a = \frac{v_0}{1 + d_0 \exp(\frac{f_t}{f_s})} \quad (6)$$

where  $f_t = -\mathbf{f}_i \cdot \hat{\mathbf{t}}$  and  $f_s$  is the stall force.  $v_0$  is the free motor velocity.

A harmonic trap of strength  $K_{\text{trap}} \geq 0$  and with center  $\mathbf{r}_o$  is applied to any monomer within a circular region of radius  $\mathcal{R}$ . The potential is:

$$V_{\text{trap}} = \frac{1}{2} K_{\text{trap}} (\mathbf{r}_i - \mathbf{r}_o)^2. \quad (7)$$

### III. SIMULATIONS

The simulations use the velocity-Verlet algorithm with a Langevin thermostat. The equation of motion for the  $i$ -th monomer is:

$$m\ddot{\mathbf{r}}_i = -\nabla U_i - \zeta \mathbf{v}_i + \boldsymbol{\eta}_i, \quad (8)$$

where  $U = V_s + V_b + V_{WCA} + V_{\text{trap}}$ ,  $\zeta$  is the friction coefficient, and  $\boldsymbol{\eta}_i$  is stochastic noise with zero mean and the variance  $\langle \boldsymbol{\eta}_i(t) \boldsymbol{\eta}_j(t') \rangle = 4k_B T \zeta \delta_{ij} \delta(t - t')$ . Temperature is set to  $k_B T = 1.0\epsilon$ , and the friction coefficient is  $\zeta = 1\sqrt{m\epsilon/\sigma^2}$ . The polymer is semi-flexible with  $\ell_p/L \approx 0.3$ . As the average dimensions of individual MPs are significantly smaller, by three to four orders of magnitude, compared to average polymer lengths in motility assays, we set the MP capture radius as  $r_c = 0.5\sigma$  with an MP density of  $\rho = 4\sigma^{-2}$ .

MPs move along the polymer with active velocity  $v_i^a$ , affected by force components along the polymer's tangent. The equation of motion for the MP includes three contributions: active velocity, tensile force  $f_t$ , and stochastic force. The MP friction coefficient is  $\zeta_{\text{MP}} = 0.1\zeta$ . Attachment and detachment occur with rates  $\kappa_{on}\delta t$  and  $\kappa_{off}\delta t$ , respectively. In our simulations we use a dimensionless Péclet number  $Pe = v_0 L^2 / D\sigma$ , where  $D = k_B T / \zeta$ , and a dimensionless rate ratio (bare processivity)  $\Omega = \kappa_{on} / (\kappa_{on} + \kappa_{off})$ . The time scale for polymer diffusion is  $\tau = L^3 \zeta / 4\sigma k_B T$ , which is used as the unit of time. Simulations run for  $10^8$  steps with the initial polymer in the trap.

### IV. RESULTS

Initially, the simulation is set up with a semiflexible polymer completely enclosed within the harmonic confinement. As shown in Fig. 1(a), the harmonic trap is modeled as a circular region on the motility assay, characterized by a trap radius of  $\mathcal{R}_{\text{trap}} = 20\sigma$ . The binding and unbinding dynamics of MPs and their directed movement along the polymer, with an active velocity characterized by the Péclet number ( $Pe$ ), induces the polymer's gliding motion. The trap, on the other hand, works to confine the polymer, resulting in a competition between the activity-driven motion and the confining force.

Our key finding is that the semi-flexible polymer in a motility assay, under the influence of a harmonic trap, exhibits predominantly two states: it can remain confined within the trap indefinitely or completely in the free state, as shown in Fig. 1(b) and (d). Once the polymer escapes the trap, it can still make frequent visits back

into the trap, but it does not remain confined for long, as the activity prevents prolonged trapping. However, we also observed states in which the polymer is transiently trapped for long durations before it escapes again. These states occur as intermediate states between completely trapped and free states. Identification of states is performed by computing the probability  $P(N_{\text{trap}})$ . For fully trapped state  $P(N_{\text{trap}} = 64)$  or  $P(N_{\text{trap}} = 0)$  for free state is always close to 1.0 except for intermediate states for which probability decreases. These states depend crucially on the trap stiffness, the activity of the MP bed characterized by  $Pe$  and  $\Omega$ , and the rigidity of the polymer.

In Fig. 2(a)-(c), we have shown the time series plot of  $N_{\text{trap}}$ , the number of trapped monomers, for three Péclet numbers at a fixed processivity of MPs and fixed rigidity of the polymer. We choose a trap strength for which the polymer is confined within the trap at  $Pe = 0$  (Fig. 2(a)). With increasing  $Pe$ , the polymer starts moving out of the trap, and we see transient jumps in the time series, which become more frequent at high  $Pe$  (Fig. 2(b-c)). We also plot the probability distribution of trapped monomers  $p(N_{\text{trap}})$  in Fig. 2(d). For smaller activities, a small peak appears at  $N_{\text{trap}} = 0$ , which means that polymer escapes the trap occasionally, while for large activities, the situation flips, leaving a small peak at  $N_{\text{trap}} = 64$ .

### A. STATE DIAGRAM

Based on these results, we constructed the state diagram for the system for various parameter values. In Fig. 3(a), we show the state diagram for varying trap strength  $K_{\text{trap}}$  and Péclet number  $Pe$  while keeping the bare processivity rate fixed at  $\Omega = 0.5$ . In the state diagram, we marked three states. In addition to fully trapped and free, we marked the state during which the polymer transiently gets trapped. The transition from the trapped to the free state is non-monotonic. The transition occurs at lower  $Pe$  values at low trap strengths as expected and occurs at progressively higher  $Pe$  with increasing  $K_{\text{trap}}$ .

To check the role of the active MP bed, in Fig. 3(b), we present the state diagram with varying  $Pe$  and  $\Omega$  for a constant trap strength  $K_{\text{trap}} = 0.08 k_B T / \sigma^2$ . At lower processivity, the polymer prefers to be trapped, and even increasing  $Pe$  cannot free the polymer. As processivity is increased, the polymer can transition to a free state with increasing  $Pe$ . This is a significant result specific to the motility assay framework. Lower processivity implies a lower on-rate or a higher off-rate. In either situation, the increase in the unbinding of the MPs allows the polymer to have multiple conformations, which is reflected in the end-to-end distribution of the polymer [12]. This further leads to a decrease in the effective bending rigidity calculated from the tangent-tangent correlations. On the other hand, an increased  $\Omega$  implies that the polymer is strongly bound by the MPs, and the conformational flexibility is much less. The effective bending rigidity is

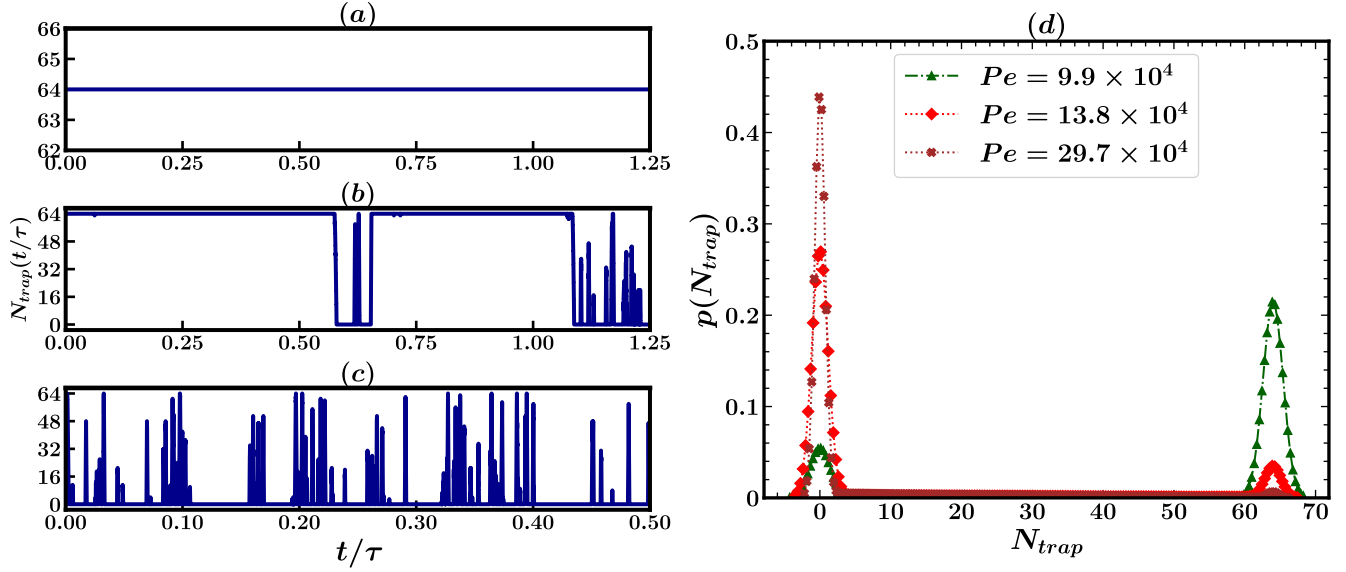


FIG. 2: Timeseries of trapped monomers  $N_{\text{trap}}$  as a function of time (expressed in units of  $\tau$ ) is shown. A semiflexible polymer of contour length  $L = 63\sigma$  with bare processivity  $\Omega = 0.5$  and persistence ratio  $\ell_p/L = 0.3$  is considered. The variation is plotted as a function of Péclet number ( $Pe$ ) while keeping the trap strength fixed at  $K_{\text{trap}} = 0.1k_B T/\sigma^2$ : (a)  $Pe = 0$ , (b)  $Pe = 17.8 \times 10^4$ , and (c)  $Pe = 29.7 \times 10^4$ . (d) Kernel density function of the number of trapped monomers,  $p(N_{\text{trap}})$ , for a semiflexible polymer with  $L = 63\sigma$  and bare processivity  $\Omega = 0.5$ . The trap strength is fixed at  $K_{\text{trap}} = 0.06k_B T/\sigma^2$ , and the trap radius is  $\mathcal{R} = 20\sigma$ . The distribution is shown for different values of Péclet number:  $Pe = 9.9 \times 10^4$ ,  $Pe = 13.9 \times 10^4$ , and  $Pe = 29.7 \times 10^4$ .

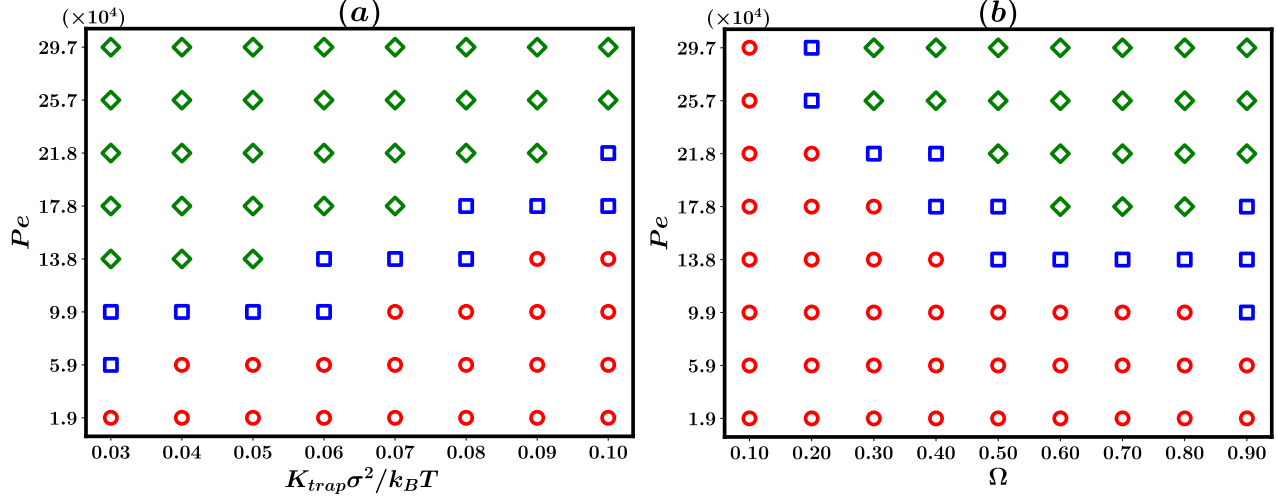


FIG. 3: Phase diagram of a polymer with contour length  $L = 63\sigma$ . The green diamonds ( $\diamond$ ) represent states where the polymer is free from the trap, while the red circles ( $\circ$ ) indicate the configurations where the polymer is trapped. The blue squares ( $\square$ ) represent the co-existence phase. The trap radius is taken to be  $\mathcal{R} = 20\sigma$ . (a) Corresponds to the scenario with bare processivity  $\Omega = 0.5$  and  $\ell_p/L = 0.30$ . (b) Illustrates the case with same persistence ratio  $\ell_p/L = 0.30$  and trap strength  $K_{\text{trap}} = 0.08 k_B T/\sigma^2$ .

higher. As we show later, reducing the bending rigidity of the polymer leads to more effective trapping of the polymer. Note that this result further corroborates the necessity to model activity in motility assays using both the tangential drive from attached MP movement and

(un)binding kinetics of individual MPs. This separation is lost when motility assays are described as active polymers with local tangential forces.

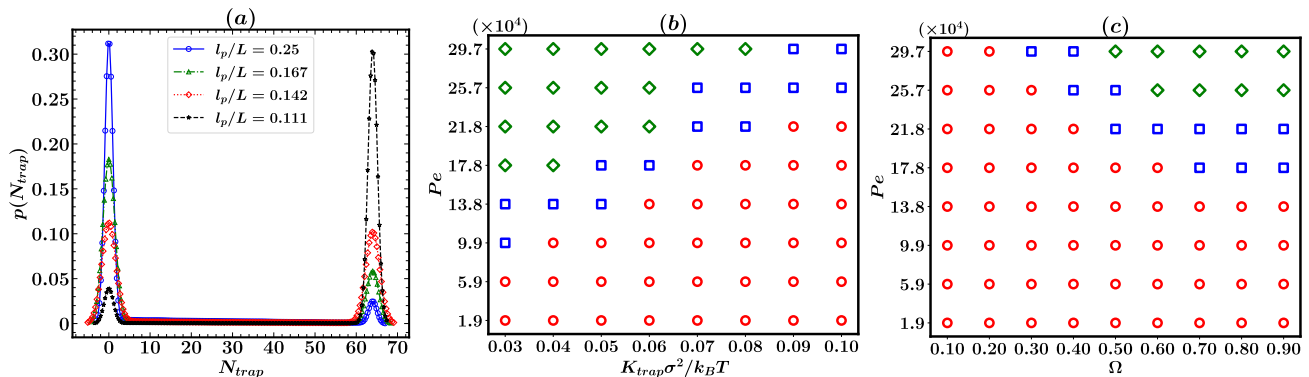


FIG. 4: (a) Probability density function  $p(N_{\text{trap}})$  of the number of trapped monomers as a function of the persistence ratio  $\ell_p/L$  for a semiflexible polymer with contour length  $L = 63\sigma$ . The trap radius is  $\mathcal{R} = 20\sigma$ , and the distribution is shown for various values of  $\ell_p/L$ , keeping the trap strength  $K_{\text{trap}} = 0.06 k_B T/\sigma^2$  and Péclet number  $Pe = 13.8 \times 10^4$  fixed. (b) Phase diagram for a polymer with  $L = 63\sigma$  and  $\mathcal{R} = 20\sigma$  as a function of both  $Pe$  and  $K_{\text{trap}}$ . The green ( $\diamond$ ) points represent states where the polymer is free from the trap, red ( $\circ$ ) points indicate configurations where the polymer is trapped, and blue ( $\square$ ) points correspond to the coexistence phase. This panel corresponds to a scenario with bare processivity  $\Omega = 0.5$  and  $\ell_p/L = 0.10$ . (c) Similar to (b), phase diagram is plotted as a function of both  $Pe$  and  $\Omega$  but with fixed trap strength  $K_{\text{trap}} = 0.08 k_B T/\sigma^2$  while maintaining the same persistence ratio  $\ell_p/L = 0.10$ .

## B. EFFECT OF RIGIDITY

Following our observations in the previous section, in Fig. 4(a), we illustrate the explicit effect of the persistence ratio,  $\ell_p/L$ , on the probability distribution of trapped monomers. The activity is kept fixed at  $Pe = 13.8 \times 10^4$ , with a confinement strength of  $K_{\text{trap}} = 0.06 k_B T/\sigma^2$  and a bare processivity rate of  $\Omega = 0.5$ . We systematically vary the persistence ratio  $\ell_p/L$ , transitioning from flexible to stiffer polymer conditions. Our results show that a flexible polymer is easily confined and requires higher activity to escape the trap. For  $\ell_p/L = 0.111$ , the polymer remains fully confined within the trap. For  $\ell_p/L = 0.143$ , the distribution  $p(N_{\text{trap}})$  shows two peaks at  $N_{\text{trap}} = 0$  and  $N_{\text{trap}} = 64$ , both of equal height, suggesting a metastable state between the trapped and escape configurations. As  $\ell_p/L$  increases further to  $\ell_p/L = 0.167$ , the peak at  $N_{\text{trap}} = 0$  becomes more pronounced, while the peak at  $N_{\text{trap}} = 64$  diminishes, indicating reduced stability in the trapped state. Finally, for  $\ell_p/L = 0.25$ , the peak at  $N_{\text{trap}} = 64$  nearly vanishes, with a strong peak at  $N_{\text{trap}} = 0$ , signifying a progressive destabilization of the trapped state as the polymer becomes stiffer.

We have also provided a detailed state diagram for a stiffer polymer  $\ell_p/L = 0.1$  in Figs. 4(b-c) to compare with Fig. 3(a-b). In both state diagrams, the trapped regime significantly increases compared to Fig. 3. The transition to a free state now requires a significantly larger  $Pe$ , i.e. a larger velocity of attached MPs.

## C. CONFINEMENT INDUCES STABLE SPIRALS

It was shown that when the activity is non-zero i.e.  $Pe \neq 0$ , the semiflexible polymer in the presence of motility assay[12] or even an active polar polymer [14] displays open chain and spiral configurations. These spirals can have both clockwise and counter-clockwise orientations. It turns out that the probability of polymer forming more turns initially increases with  $Pe$  and then decreases for a higher value of  $Pe$ [11]. To determine how many turns these spirals take, we use an order parameter called the turning number which is defined as

$$\psi_i = \frac{1}{2\pi} \sum_{j=1}^{i-1} [\phi_{j+1} - \phi_j]$$

where  $\phi_j$  is defined by  $\hat{t}_j = (\cos \phi_j, \sin \phi_j)$ , and  $\phi_{j+1} - \phi_j$  gives the angle increment between consecutive bonds[11]. Thus  $\psi_N$ , quantifies the number of turns the polymer undergoes from one end to the other. For a straight chain,  $\psi_N = 0$ , while for a single loop,  $\psi_N = \pm 1$  for clockwise/anticlockwise turns, with the magnitude of  $\psi_N$  increasing for multiple turns, indicating a spiral conformation. The value of  $\psi_N$  depends primarily on the polymer's length and is measured at steady state.

In Fig. 5(a), we show the distribution of  $\psi_N$ ,  $p(\psi_N)$ , for three  $Pe$  values without a trap ( $K_{\text{trap}} = 0$ ). At  $Pe = 5.9 \times 10^4$ , a central peak near  $\psi_N \approx 0$  indicates open-chain glide motion, with secondary peaks at  $\psi_N \approx \pm 2.5$  corresponding to unstable spirals. At  $Pe = 9.9 \times 10^4$ , the central peak remains, but two new spiral peaks appear at  $\psi_N \approx \pm 3$ . As  $Pe$  increases to  $13.8 \times 10^4$ , the central peak diminishes, signaling the instability of open-chain motion, and stable spirals form at  $\psi_N \approx \pm 3$ . At

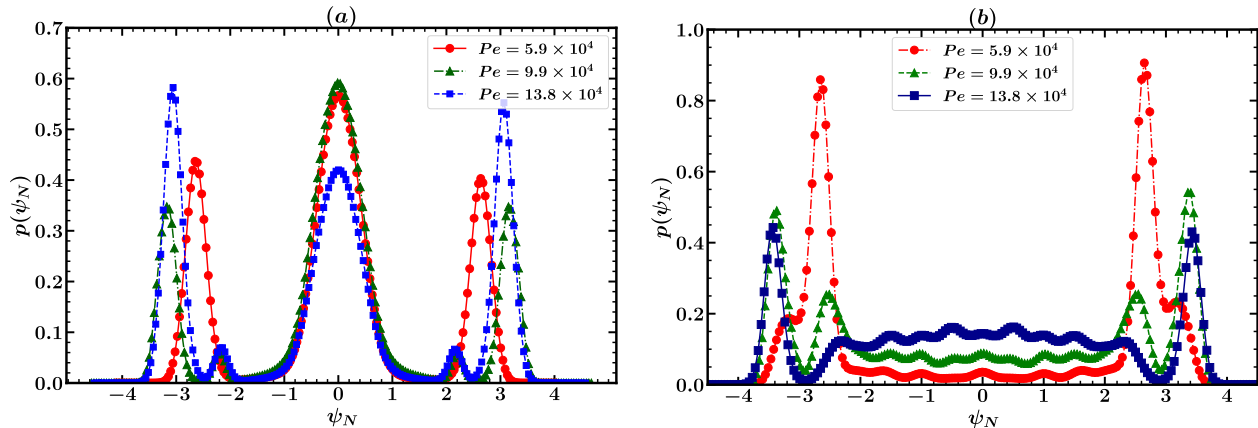


FIG. 5: Steady-state probability distributions of the turning number for different values of  $Pe$ :  $5.9 \times 10^4$ ,  $9.9 \times 10^4$ , and  $13.8 \times 10^4$ . The trap radius is set to  $\mathcal{R} = 20\sigma$ , and the semiflexible polymer length is  $L = 63\sigma$ . The bare processivity is  $\Omega = 0.5$ . The trap strength is varied as follows: (a)  $K_{\text{trap}} = 0$  and (b)  $K_{\text{trap}} = 0.4 k_{\text{B}}T/\sigma^2$ .

higher  $Pe$ , the spirals lose stability, marking a re-entrant transition [11].

When a harmonic trap is applied ( $K_{\text{trap}} = 0.4 k_{\text{B}}T/\sigma^2$ ), with  $Pe$  chosen so that the polymer stays within the trap, the impact on spiral formation is shown in Fig. 5(b). The gliding motion is halted, eliminating the central peak. At  $Pe = 5.9 \times 10^4$ , two stable spirals emerge at  $\psi_N \approx \pm 3$  with larger stability as compared to  $K_{\text{trap}} = 0$ . As  $Pe$  increases to  $9.9 \times 10^4$ , stable spirals appear at  $\psi_N \approx \pm 2.5$  and  $\psi_N \approx \pm 3.5$ . At  $Pe = 13.8 \times 10^4$ , the peak at  $\psi_N \approx \pm 2.5$  disappears, leaving a single peak at  $\psi_N \approx \pm 3.5$ , nearly identical to the peak at  $Pe = 9.9 \times 10^4$ .

#### D. DYNAMICS OF CENTER OF MASS

The mean square displacement (MSD) of the centre of mass of a polymer demonstrates the trapping-untrapping transition. The MSD is defined as  $MSD(\Delta t) = \langle (\mathbf{r}_{\text{cm}}(t + \Delta t) - \mathbf{r}_{\text{cm}}(t))^2 \rangle$ , where  $\mathbf{r}_{\text{cm}}(t)$  represents the polymer's centre of mass position at time  $t$ . As the trap strength increases, the polymer becomes more confined within the trap, competing with the polymer's activity, characterized by the Péclet number  $Pe$ .

In the absence of a trap, the MSD as a function of time lag ( $\Delta t/\tau$ ) reveals three distinct regimes depending on the value of  $Pe$ . For  $Pe = 1.9 \times 10^4$ , as shown in Fig. 6(a), three behaviours are observed: (1) a diffusive regime ( $MSD \propto \Delta t/\tau$ ) for  $\Delta t/\tau \lesssim 10^{-3}$ , (2) a ballistic regime ( $MSD \propto (\Delta t/\tau)^2$ ) for intermediate times, and (3) a return to diffusive behaviour for  $\Delta t/\tau \gtrsim 10^{-1}$ . Increasing the activity parameter to  $Pe = 9.9 \times 10^4$  eliminates the initial diffusive regime, leaving a ballistic regime at  $\Delta t/\tau \lesssim 10^{-2}$ , followed by diffusive behaviour. At an even higher  $Pe = 25.7 \times 10^4$ , a similar two-regime pattern persists, demonstrating how increasing activity alters the dynamics of the polymer. An analogous se-

quence comprising diffusive, ballistic and then diffusive behaviours have been observed in the case of individual active Brownian particles [45–47].

Introducing a weak trap ( $K_{\text{trap}} = 0.1 k_{\text{B}}T/\sigma^2$ ) alters the MSD significantly. For  $Pe = 1.9 \times 10^4$ , the long-range center of mass diffusion is suppressed by the trap, with the MSD saturating to a constant value for  $\Delta t/\tau > 10^{-3}$ . However, at shorter times ( $\Delta t/\tau < 10^{-3}$ ), a diffusive regime is still observed. For moderately higher activity ( $Pe = 9.9 \times 10^4$ ), the MSD exhibits diffusive behaviour up to  $\Delta t/\tau \approx 10^{-3}$ , followed by saturation accompanied by oscillations, likely induced by activity effects on the polymer [48]. For large activity ( $Pe = 25.7 \times 10^4$ ), the polymer escapes the trap, leading to a ballistic regime up to  $\Delta t/\tau \approx 10^{-3}$  before transitioning to diffusive behavior.

A stronger trap ( $K_{\text{trap}} = 0.5 k_{\text{B}}T/\sigma^2$ ) suppresses diffusion at longer times, regardless of  $Pe$ . Within the diffusive regime, the MSD increases with  $Pe$ , reflecting the enhanced space exploration within the trap facilitated by increased activity. Additionally, for cases where MPs attach more with the polymer (high value of  $\Omega$ ), oscillations in the MSD are observed, but their amplitude decreases with increasing  $Pe$ , contrasting the behavior of underdamped Brownian particles in traps [48]. The reduction in amplitude might result from the boundary effect, where at large activity, the polymer encounters the trap's boundary, potentially suppressing the oscillations. These results are summarized in Fig. 6(c), providing insight into the interplay between trap strength and activity in determining polymer dynamics.

#### E. EXCESS KURTOSIS

A motility assay inherently drives the system out of equilibrium at all times. Harmonic confinement may or may not alter the system's nonequilibrium state. To in-

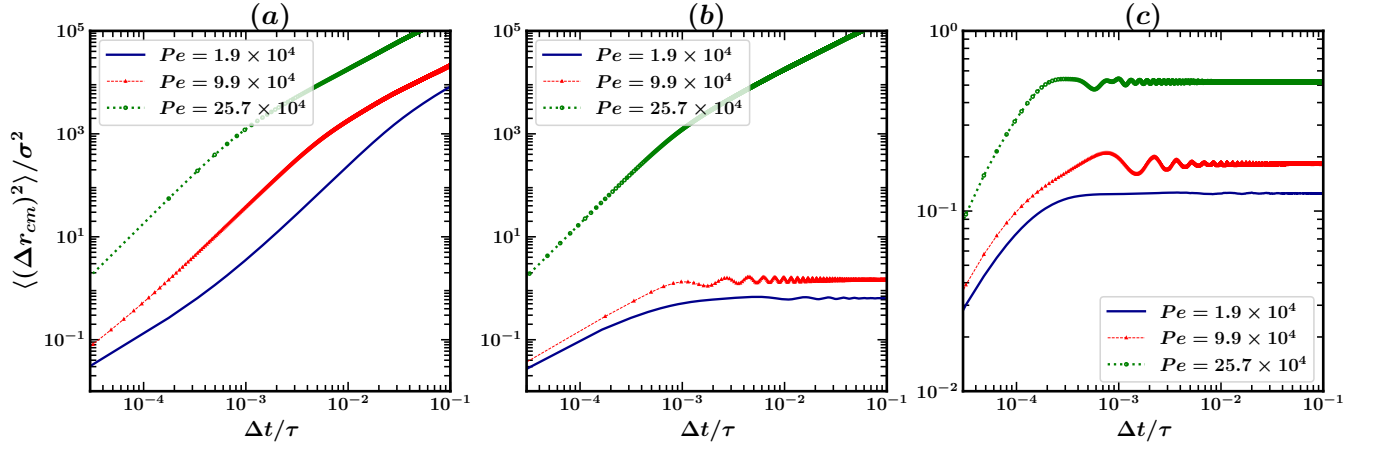


FIG. 6: Mean squared displacement (MSD) of the centre of mass of a semiflexible polymer with contour length  $L = 63\sigma$  in the presence of a harmonic trap with radius  $\mathcal{R} = 20\sigma$  and bare processivity  $\Omega = 0.5$ . The variation of MSD is shown for three different Péclet numbers,  $Pe = 1.9 \times 10^4$ ,  $Pe = 9.9 \times 10^4$ , and  $Pe = 25.7 \times 10^4$ , across three different trap strengths: (a)  $K_{\text{trap}} = 0$ , (b)  $K_{\text{trap}} = 0.1 k_{\text{B}}T/\sigma^2$ , and (c)  $K_{\text{trap}} = 0.5 k_{\text{B}}T/\sigma^2$ .

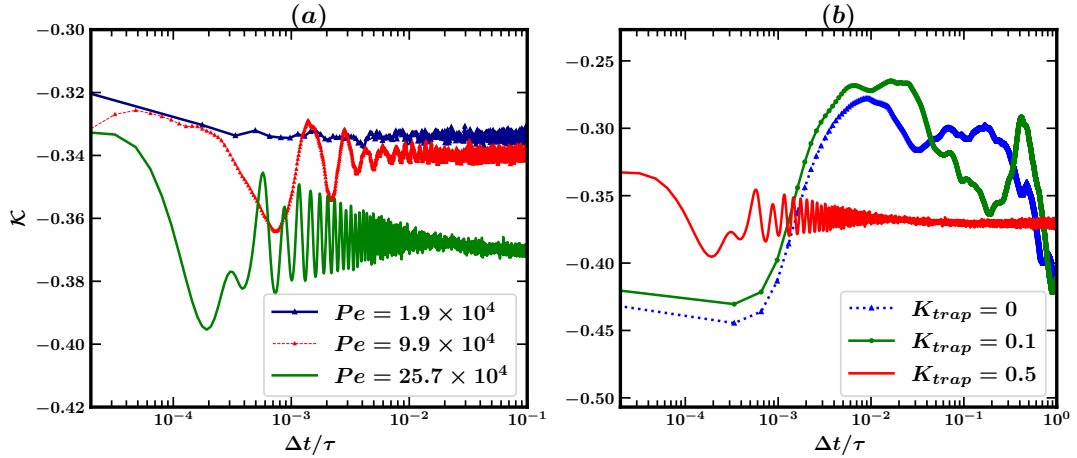


FIG. 7: Excess kurtosis ( $\mathcal{K}$ ) of the center of mass of a semiflexible polymer with contour length  $L = 63\sigma$  in the presence of a harmonic trap of radius  $\mathcal{R} = 20\sigma$  and bare processivity  $\Omega = 0.8$ . (a) Variation of  $\mathcal{K}$  for a fixed trap strength  $K_{\text{trap}} = 0.5 k_{\text{B}}T/\sigma^2$  and three different Péclet numbers:  $Pe = 1.9 \times 10^4$ ,  $9.9 \times 10^4$ , and  $25.7 \times 10^4$ . (b) Variation of  $\mathcal{K}$  for a fixed Péclet number  $Pe = 25.7 \times 10^4$  under three different trap strengths:  $K_{\text{trap}} = 0, 0.1, \text{ and } 0.5 k_{\text{B}}T/\sigma^2$ .

investigate this, the excess kurtosis of the polymer emerges as a suitable diagnostic measure. If  $\mathbf{r}_{\text{cm}}$  denotes the position of the centre of mass, excess kurtosis  $\mathcal{K}$  is defined as

$$\mathcal{K} = \frac{\langle r_{\text{cm}}^4 \rangle}{3\langle r_{\text{cm}}^2 \rangle^2} - 1.$$

For a normal distribution (and hence for the equilibrium case),  $\mathcal{K} = 0$ . Any deviation from zero indicates nonequilibrium behaviour.

Figure 7(a) shows the trend of excess kurtosis of the centre of mass (COM) under a strong confinement potential  $K_{\text{trap}} = 0.5 k_{\text{B}}T/\sigma^2$ . For all nonzero values of  $Pe$ , the kurtosis exhibits negative value saturation, signifying non-Gaussian behaviour even for small activity lev-

els, such as  $Pe = 1.9 \times 10^4$ . For slightly higher activity ( $Pe = 9.9 \times 10^4$ ), oscillations appear in an intermediate time regime  $10^{-3} \leq \Delta t/\tau \leq 10^{-2}$ . The frequency and the amplitude of these oscillations increase with higher activity ( $Pe = 25.7 \times 10^4$ ). These oscillations result from the interplay between activity and confinement: the activity drives the polymer outward, creating a transient heavy-tailed distribution (high kurtosis), while the confinement counteracts this, leading to a more compact distribution (low kurtosis). As activity increases,  $\mathcal{K}$  saturates at even lower negative values, suggesting that the confinement dominates at long times, smoothing out the effect of activity and resulting in a stationary distribution.

Figure 7(b) illustrates the effect of the confinement

potential on kurtosis for a fixed activity value of  $Pe = 25.7 \times 10^4$ . In the absence of confinement, the polymer freely moves on the gliding assay, producing a non-monotonic kurtosis profile. At shorter times, the polymer exhibits gliding motion, while at later times, spiral-like motions dominate, leading to a reduction in kurtosis. For a weak confinement potential ( $K_{\text{trap}} = 0.1 k_B T / \sigma^2$ ), the polymer remains mostly free but occasionally encounters the trap, hindering its motion and affecting the kurtosis. For stronger confinement ( $K_{\text{trap}} = 0.5 k_B T / \sigma^2$ ), the polymer becomes fully trapped. Similarly to the previous case, the system transitions to a stationary state through oscillations.

## V. CONCLUSIONS

In this paper, we studied the effect of a harmonic trap on a semiflexible polymer embedded in a motility assay, where MPs stochastically bind, unbind, and walk along the polymer. Using Langevin dynamics simulations, we have constructed a detailed state diagram that highlights a two-state transition of the polymer from a trapped to a free state, with an intermediate co-existence region. Our findings reveal that the trapping of the polymer is influenced not only by the interplay between activity ( $Pe$ ) and trap strength ( $K_{\text{trap}}$ ) but also by the polymer stiffness, characterized by the persistence ratio  $l_p/L$ . We showed that decreasing the stiffness of the polymer supports more trapped states and shifts the trapped region to larger Péclet numbers in the state diagram, which means flexible polymers require larger activity to transit from the trapped state to the free state. We have also shown that confinement induces the polymer to adopt spiral conformations with various turning numbers, exhibiting both clockwise and counterclockwise

orientations. The effect of the trap on the polymer is also shown to be reflected in the centre of mass diffusion and kurtosis. Interestingly, we found that for active polymers, the amplitude of oscillations in the dynamics of the centre of mass decreases with increasing activity, that is, with the Péclet number.

One of the interesting outcomes of our study is that rigidity shifts the barrier that separates trapping and untrapping regimes in the state diagram. Therefore, this study emphasizes the crucial role of polymer rigidity in harmonic trapping applied to motility assays. Because polymers in motility assays simulate the natural intracellular environment of many biofilaments, understanding their behaviour when confined is crucial for numerous biophysical studies. An effective method to confine biofilaments is through optical trapping, frequently employed in biological filament motor systems as an essential tool for manipulating and measuring forces. For instance, using optical trapping, it is shown that the force generated by a few growing parallel-acting filaments is about 1 pN [49]. The method has also been used to trap whole cells [50, 51].

Although the study offers qualitative insight into the combined impact of polymer rigidity, activity, and confinement, complementary motility assay experiments using optical tweezers would offer a more comprehensive understanding. Such experiments would illuminate the complex dynamical behaviour of semi-flexible polymers under harmonic trapping within an active environment.

## VI. ACKNOWLEDGMENTS

SR and AKD thank Abhishek Chaudhuri for valuable suggestions and a critical reading of the manuscript.

- 
- [1] F. Gittes, B. Mickey, J. Nettleton, and J. Howard, Flexural rigidity of microtubules and actin filaments measured from thermal fluctuations in shape., *The Journal of cell biology* **120**, 923 (1993).
  - [2] D. C. Yadufashije, Lecture notes: Cell biology, Lecture Notes: Cell Biology (April 19, 2018). *Lecture Notes: Cell Biology* (2018).
  - [3] J. Howard and R. Clark, Mechanics of motor proteins and the cytoskeleton, *Appl. Mech. Rev.* **55**, B39 (2002).
  - [4] N. Chaffey, Alberts, b., johnson, a., lewis, j., raff, m., roberts, k. and walter, p. *molecular biology of the cell*. 4th edn. (2003).
  - [5] Y. Harada and T. Yanagida, Direct observation of molecular motility by light microscopy, *Cell Motility and the Cytoskeleton* **10**, 71 (1988).
  - [6] J. Howard, A. Hudspeth, and R. Vale, Movement of microtubules by single kinesin molecules, *Nature* **342**, 154 (1989).
  - [7] L. Bourdieu, T. Duke, M. Elowitz, D. Winkelmann, S. Leibler, and A. Libchaber, Spiral defects in motility assays: a measure of motor protein force, *Physical review letters* **75**, 176 (1995).
  - [8] T. Duke, T. E. Holy, and S. Leibler, "gliding assays" for motor proteins: A theoretical analysis, *Physical review letters* **74**, 330 (1995).
  - [9] J. M. Scholey, *Motility assays for motor proteins* (Academic Press, 1993).
  - [10] A. Chaudhuri and D. Chaudhuri, Forced desorption of semiflexible polymers, adsorbed and driven by molecular motors, *Soft Matter* **12**, 2157 (2016).
  - [11] A. Shee, N. Gupta, A. Chaudhuri, and D. Chaudhuri, A semiflexible polymer in a gliding assay: Reentrant transition, role of turnover and activity, *Soft Matter* **17**, 2120 (2021).
  - [12] N. Gupta, A. Chaudhuri, and D. Chaudhuri, Morphological and dynamical properties of semiflexible filaments driven by molecular motors, *Physical Review E* **99**, 042405 (2019).
  - [13] T. Q. Uyeda, S. J. Kron, and J. A. Spudich, Myosin step size: estimation from slow sliding movement of actin over low densities of heavy meromyosin, *Journal of molecular biology* **214**, 699 (1990).



- [14] R. E. Isele-Holder, J. Elgeti, and G. Gompper, Self-propelled worm-like filaments: spontaneous spiral formation, structure, and dynamics, *Soft matter* **11**, 7181 (2015).
- [15] A. Khosravanizadeh and S. Dmitrieff, Rotation-beating dynamics of a driven flexible filament: role of motor protein properties, arXiv preprint arXiv:2409.12729 (2024).
- [16] R. Chelakkot, M. F. Hagan, and A. Gopinath, Synchronized oscillations, traveling waves, and jammed clusters induced by steric interactions in active filament arrays, *Soft matter* **17**, 1091 (2021).
- [17] I. Tiwari, P. Parmananda, and R. Chelakkot, Periodic oscillations in a string of camphor infused disks, *Soft Matter* **16**, 10334 (2020).
- [18] S. K. Anand, R. Chelakkot, and S. P. Singh, Beating to rotational transition of a clamped active ribbon-like filament, *Soft matter* **15**, 7926 (2019).
- [19] O. Dauchot and V. Démery, Dynamics of a self-propelled particle in a harmonic trap, *Physical review letters* **122**, 068002 (2019).
- [20] K. Malakar, A. Das, A. Kundu, K. V. Kumar, and A. Dhar, Steady state of an active brownian particle in a two-dimensional harmonic trap, *Physical Review E* **101**, 022610 (2020).
- [21] D. Chaudhuri and A. Dhar, Active brownian particle in harmonic trap: exact computation of moments, and re-entrant transition, *Journal of Statistical Mechanics: Theory and Experiment* **2021**, 013207 (2021).
- [22] M. Hennes, K. Wolff, and H. Stark, Self-induced polar order of active brownian particles in a harmonic trap, *Physical review letters* **112**, 238104 (2014).
- [23] I. Santra, U. Basu, and S. Sabhapandit, Direction reversing active brownian particle in a harmonic potential, *Soft Matter* **17**, 10108 (2021).
- [24] D. Wexler, N. Gov, K. Ø. Rasmussen, and G. Bel, Dynamics and escape of active particles in a harmonic trap, *Physical review research* **2**, 013003 (2020).
- [25] J. A. Spudich, S. E. Rice, R. S. Rock, T. J. Purcell, and H. M. Warrick, Optical traps to study properties of molecular motors, *Cold Spring Harbor Protocols* **2011**, pdb (2011).
- [26] C. Bustamante, L. Alexander, K. Maciuba, and C. M. Kaiser, Single-molecule studies of protein folding with optical tweezers, *Annual review of biochemistry* **89**, 443 (2020).
- [27] R. Bar-Ziv, E. Moses, and P. Nelson, Dynamic excitations in membranes induced by optical tweezers, *Biophysical journal* **75**, 294 (1998).
- [28] A. J. Merz, M. So, and M. P. Sheetz, Pilus retraction powers bacterial twitching motility, *Nature* **407**, 98 (2000).
- [29] D. E. Dupuis, W. H. Guilford, J. Wu, and D. Warshaw, Actin filament mechanics in the laser trap, *Journal of Muscle Research & Cell Motility* **18**, 17 (1997).
- [30] A. Mishra, T. Maltais, T. Walter, A. Wei, S. Williams, and S. Wereley, Trapping and viability of swimming bacteria in an optoelectric trap, *Lab on a Chip* **16**, 1039 (2016).
- [31] J. M. Nascimento, L. Z. Shi, C. Chandsawangbhuwana, J. Tam, B. Durrant, E. L. Botvinick, and M. W. Berns, Use of laser tweezers to analyze sperm motility and mitochondrial membrane potential, *Journal of Biomedical Optics* **13**, 014002 (2008).
- [32] J. Mateos-Langerak, M. Bohn, W. De Leeuw, O. Giromus, E. M. Manders, P. J. Verschure, M. H. Indemans, H. J. Gierman, D. W. Heermann, R. Van Driel, *et al.*, Spatially confined folding of chromatin in the interphase nucleus, *Proceedings of the National Academy of Sciences* **106**, 3812 (2009).
- [33] F. Brochard and P.-G. de Gennes, Dynamics of confined polymer chains, *The Journal of Chemical Physics* **67**, 52 (1977).
- [34] C. Cordeiro, M. Molisana, and D. Thirumalai, Shape of confined polymer chains, *Journal de Physique II* **7**, 433 (1997).
- [35] D. K. Lubensky and D. R. Nelson, Driven polymer translocation through a narrow pore, *Biophysical journal* **77**, 1824 (1999).
- [36] K. Luo, T. Ala-Nissila, S.-C. Ying, and A. Bhattacharya, Influence of polymer-pore interactions on translocation, *Physical Review Letters* **99**, 148102 (2007).
- [37] J. A. Cohen, A. Chaudhuri, and R. Golestanian, Stochastic sensing of polynucleotides using patterned nanopores, *Physical Review X* **2**, 021002 (2012).
- [38] R. Kumar, A. Chaudhuri, and R. Kapri, Sequencing of semiflexible polymers of varying bending rigidity using patterned pores, *The Journal of chemical physics* **148** (2018).
- [39] G. Upadhyay, R. Kapri, A. K. Dasanna, and A. Chaudhuri, Packing and ejection dynamics of polymers: Role of confinement, polymer stiffness and activity, arXiv preprint arXiv:2407.18872 (2024).
- [40] L. Florin, C. Sapp, R. E. Streeck, and M. Sapp, Assembly and translocation of papillomavirus capsid proteins, *Journal of virology* **76**, 10009 (2002).
- [41] A. Rahmani, C. Castelnovo, J. Schmit, and C. Chamon, Dynamics of single polymers under extreme confinement, *Journal of Statistical Mechanics: Theory and Experiment* **2007**, P09022 (2007).
- [42] L. D. Landau and E. M. Lifshitz, *Statistical Physics: Volume 5*, Vol. 5 (Elsevier, 2013).
- [43] A. Huang, A. Bhattacharya, and K. Binder, Conformations, transverse fluctuations, and crossover dynamics of a semi-flexible chain in two dimensions, *The Journal of Chemical Physics* **140** (2014).
- [44] G. I. Bell, Models for the specific adhesion of cells to cells: a theoretical framework for adhesion mediated by reversible bonds between cell surface molecules., *Science* **200**, 618 (1978).
- [45] J. R. Howse, R. A. Jones, A. J. Ryan, T. Gough, R. Vafabakhsh, and R. Golestanian, Self-motile colloidal particles: from directed propulsion to random walk, *Physical review letters* **99**, 048102 (2007).
- [46] K. Martens, L. Angelani, R. Di Leonardo, and L. Bocquet, Probability distributions for the run-and-tumble bacterial dynamics: An analogy to the lorentz model, *The European Physical Journal E* **35**, 1 (2012).
- [47] C. Bechinger, R. Di Leonardo, H. Löwen, C. Reichardt, G. Volpe, and G. Volpe, Active particles in complex and crowded environments, *Reviews of modern physics* **88**, 045006 (2016).
- [48] M. Patel and D. Chaudhuri, Exact moments for trapped active particles: inertial impact on steady-state properties and re-entrance, arXiv preprint arXiv:2404.01107 (2024).
- [49] M. J. Footer, J. W. Kerssemakers, J. A. Theriot, and M. Dogterom, Direct measurement of force generation by actin filament polymerization using an optical trap, *Proceedings of the National Academy of Sciences* **104**, 2181 (2007).

- [50] M.-C. Zhong, X.-B. Wei, J.-H. Zhou, Z.-Q. Wang, and Y.-M. Li, Trapping red blood cells in living animals using optical tweezers, *Nature communications* **4**, 1768 (2013).
- [51] G. Volpe, G. P. Singh, and D. Petrov, Dynamics of a growing cell in an optical trap, *Applied Physics Letters* **88** (2006).